Journal of the Physical Society of Japan
Vol. 76, No. 8, August, 2007, 083704

Observation of Spin–Orbit Berry's Phase in Magnetoresistance of a Two-Dimensional Hole Anti-dot System

Ning KANG*, Eisuke ABE, Yoshiaki HASHIMOTO,
Yasuhiro IYE, and Shingo KATSUMOTO

Institute for Solid State Physics, University of Tokyo,
5-1-5 Kashiwanoha, Kashiwa, Chiba 277-8581

(Received April 5, 2007; accepted July 2, 2007; published August 10, 2007)

We report a study of the Aharonov–Bohm (AB) type oscillation of weak field magnetoresistance in an anti-dot lattice (ADL) of a two-dimensional hole system in the presence of strong spin–orbit interaction. The Fourier transform of the oscillations reveals non-monotonic evolutions with the different range of harmonic component, which are indicative of the existence of additional phase factors. A simulation considering Berry's phase and the phase arising from the spin–orbit shift in the momentum space shows qualitative agreement with the experiment.

KEYWORDS: spin–orbit interaction, Berry's phase, Aharonov–Bohm effect
DOI: 10.1143/JPSJ.76.083704

Spin–orbit interaction in two-dimensional (2D) system is predicted to introduce an additional geometric phase (Berry's phase).[1–5] Here we consider the case of 2D hole system (2DHS), in which the spin–orbit interaction is strong in III–V compound semiconductors due to the p-orbital nature of the valence bands. In a 2DHS with the Rashba-type spin–orbit coupling, the additional phase shifts arise in two ways. The spin–orbit interaction causes split of the parabolic dispersion, producing two Fermi circles of opposite spins [Figs. 1(a), 1(b)].[6–11] This means, the hole system has two different Fermi wave vectors, the difference of which (Δk_F) gives a phase shift and modifies the interference through, e.g., a ring structure. Another shift in phase comes from the spin part of the wavefunction. When a hole moves along a closed contour in the real space, the same occurs in k-space and it feels effective magnetic field B_{eff} due to the spin–orbit interaction. B_{eff} is in the 2D plane and orthogonal to the velocity. Hence when B_{eff} is strong enough, the spin turns by 2π in the 2D plane, and acquires Berry's phase of 0 or π.

When an external magnetic field B_{ext} is applied perpendicular to the 2DHS plane, the hole moving along a loop acquires an Aharonov–Bohm (AB) phase. At the same time, the in-plane spin-component diminishes [Fig. 1(c)]. This hence affects the above two additional phases. The variation in Berry's phase ($\Delta\theta_B$) and that in the phase due to Δk_F ($\Delta\theta_k$) are given as[1–5,13]

$$\Delta\theta_B = \pi(1 - \cos\theta), \quad (1)$$

$$\Delta\theta_k = \pi r \Delta k_F \sin\theta, \quad (2)$$

where $\theta \equiv \arctan(B_{eff}/B_{ext})$, and r is the radius of the AB ring. Though significant warping of the outer Fermi contour is reported[6,7] as shown in Fig. 1(b), we can consider Δk_F as an average over the perimeter in the present discussion. Hence the phase of an AB oscillation in a ring made of such 2DHG should show continuous shift giving a nontrivial peak shape in its Fourier transform (FT) amplitude versus the frequency when the FT is performed in a finite field range. In experiments, such phases have been observed as splitting of AB magnetoresistance (MR) oscillation frequency in single AB rings.[12–14] Especially the authors of ref. 13 observed nontrivial variation of the main FT peak due to the phase shift represented in eqs. (1) and (2).

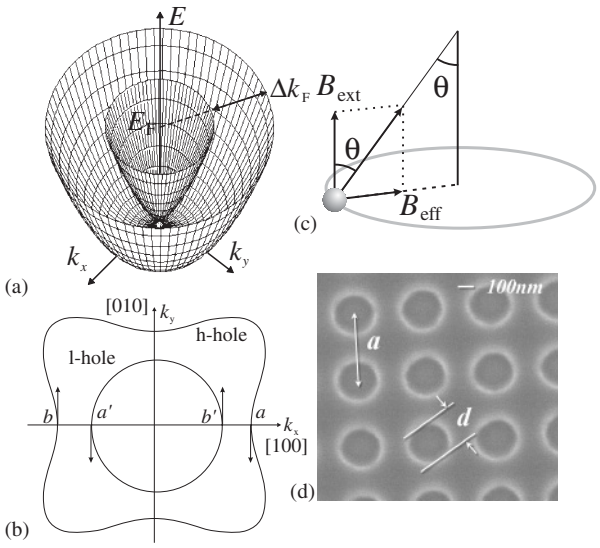

Fig. 1. (a) Surface plot of spin subbands explains two Fermi contours with different k_F appear as a result of spin–orbit interaction. (b) According to more realistic calculation,[6,7] the outer subband (h-hole) is significantly warped. The points marked a, a', b, b' with the indications of spin directions are to give possible examples of l-hole–h-hole mixing (see text). (c) Schematic illustration of B_{eff} seen by holes moving around a ring structure in the presence of spin–orbit interaction. (d) Scanning electron micrograph of the ADL sample.

In an anti-dot structure, the carriers are excluded from a dot region and MR oscillation similar to that in an AB ring is expected. In an anti-dot lattice (ADL), AB oscillations of paths around single anti-dots should be averaged out because of random phasing, whereas the effect of the AB phase remains in the density of states. The resulting MR oscillation is called an AB-type oscillation.[15–18] It is, then, of strong interest whether the effect of spin–orbit Berry's phase appears in the AB-type oscillation.

In this letter, we report observation of the predicted Berry's phase through clear splitting of the main peak in FT

*E-mail: ning.kang@issp.u-tokyo.ac.jp

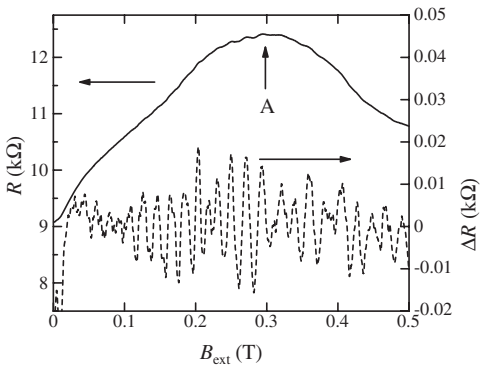

Fig. 2. Upper solid line: Resistance of the sample as a function of the external magnetic field B_{ext} for $T = 60$ mK. Lower broken line: Extracted oscillating part of the MR. For the background subtraction, a 12th order polynomial for each set of 100 consecutive data points is adopted.

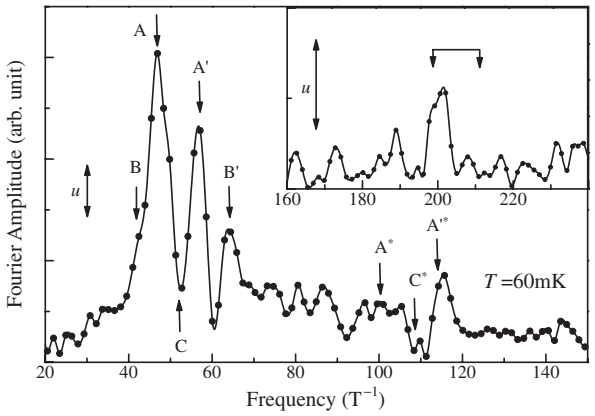

Fig. 3. Fourier spectrum of the AB-type oscillation in the MR at 60 mK. The main peak splits into four (B, A, A′, B′) and also the 2nd harmonic splits into two (A*, A′*). (The other two are within the noise level.) The inset shows peak structures around four times frequency of the main peak structure as indicated by arrows. The scales of FT amplitude are shown by the arrows marked as u in the respective figures.

of the AB-type oscillation in the MR of an ADL. The shift in k-space is independently estimated from the Shubnikov–de Haas (SdH) oscillation. Because the ADL automatically performs the disorder average, random specific effects in h/e oscillation are suppressed and intrinsic information can be obtained.

An (Al,Ga)As/GaAs heterostructure was grown by molecular beam epitaxy on a (001) GaAs substrate. Delta-doped Be layers produced a 2DHS with the hole concentration of $2.3 \times 10^{11}\,\mathrm{cm}^{-2}$ and the mobility of $6.8 \times 10^{4}\,\mathrm{cm}^2/(\mathrm{V\,s})$ at 4.2 K. SdH oscillation in the MR of the 2DHS without ADL was measured at 60 mK. From the plot of the peak index versus the inverse magnetic field, the concentrations of holes with smaller Fermi contour and larger one as 0.78×10^{11} and $1.56 \times 10^{11}\,\mathrm{cm}^{-2}$ respectively. In this letter, we call the former and the latter as l-holes and h-holes, respectively. In the simple effective mass model, these two spin-split hole bands correspond to the two Fermi contours in Fig. 1(a), though significant warping in h-hole band is reported in more realistic band calculation.[6,7] The grown film was wet-etched into Hall bars with [110] current direction. Circular anti-dot shape is adopted and ADLs were defined by electron beam lithography and wet-etching to a depth of 50 nm. An ADL is characterized mainly by the dot diameter d, the lattice structure, and the lattice period a. In this study, we designed a square lattice aligned along [110] ([$\bar{1}$10]) with $d = 250$ nm and $a = 500$ nm [see Fig. 1(d)].

The sample was directly immersed in ^{3}He–^{4}He mixture in a mixing chamber of a dilution refrigerator and cooled down to 60 mK. B_{ext} up to 6 T was applied by a superconducting solenoid. The resistance was measured in four-terminal configuration by standard lock-in technique with a frequency of 80 Hz.

The solid line in Fig. 2 shows the resistance of the sample as a function of B_{ext} up to 0.5 T. In higher field region, formation of the edge states and alignment of hole spins perpendicular to the plane bring about different physics. Therefore, we deal mainly with this low-field region. The MR shows a clear commensurability peak marked as A by an arrow in the Fig. 2. Generally such peaks in resistance appear when the carrier cyclotron orbits are commensurate with an ADL and localized in the lattice. For a circular Fermi contour, the classical cyclotron radius R_c is expressed as $\hbar k_F/eB_{ext}$, where the Fermi wavevector k_F is written as $\sqrt{4\pi p}$ with the hole concentration p (here we assume the spin degeneracy is lifted). B_{ext} at peak position A in Fig. 2 can be well ascribed to localized orbits of l-hole encircling single anti-dot. For h-hole, as noted above, we should take into account the effect of warped Fermi contour in Fig. 1(b).

As shown in Fig. 2, an oscillation with a short period superposed on the commensurability peak is visible. In order to extract the oscillating component, we subtract the background commensurability structure by fitting slowly-varying functions. An example of extracted resistance variation is shown with the broken line in Fig. 2, which exhibits a clear fast oscillation. Here for the background subtraction, a 12th order polynomial for each set of 100 consecutive data points is adopted. Although the selection of fitting function affects the outlook of the oscillatory component, little is affected in the main and sub peak structures in the Fourier space.

The observed oscillations are nearly periodic in B_{ext}. The SdH oscillation is not visible in this field range due to the restriction of the space for free cyclotron motion. The FT amplitude of the extracted oscillation is displayed in Fig. 3. The magnetic field range is taken from -0.5 to 0.5 T. At the main peak around $50\,\mathrm{T}^{-1}$, clear splitting into three sub-peaks, marked as A, A′, and B′, is observed. Sub-peak A has a shoulder structure at lower frequency marked as B. From the positions of peaks A, A′, and B′, and a shoulder B, the center of the main peak structure is determined to be $52\,\mathrm{T}^{-1}$, where a sharp dip marked as C is located. If we measure the oscillation frequency with the magnetic flux on the circle with radius $a/2$, position C just corresponds to the flux quantum h/e, confirming that the peak structure originates from the AB effect around single anti-dots through the modulation in the density of states.

As noted above, the selection of functional form for background subtraction does not affect the characteristics shown in Fig. 3 as long as the fitting function is slowly varying versus B_{ext}.

Another characteristic structure in Fig. 3 is a dip-peak structure around $108\,\mathrm{T}^{-1}$ marked as C*, which corresponds

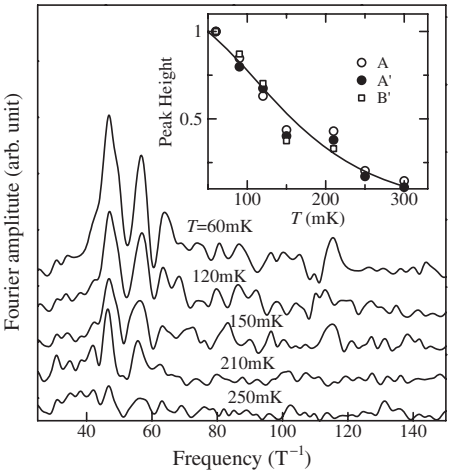

Fig. 4. FT results at temperatures from 300 down to 60 mK. The data are offset for clarity. The inset shows the peak heights normalized at 60 mK for peaks A, A′, and B′. (As for the peak B′, the data points above 210 mK are not plotted since they are comparable with the background.) The solid line in the inset is the fit to the Dingle function (3).

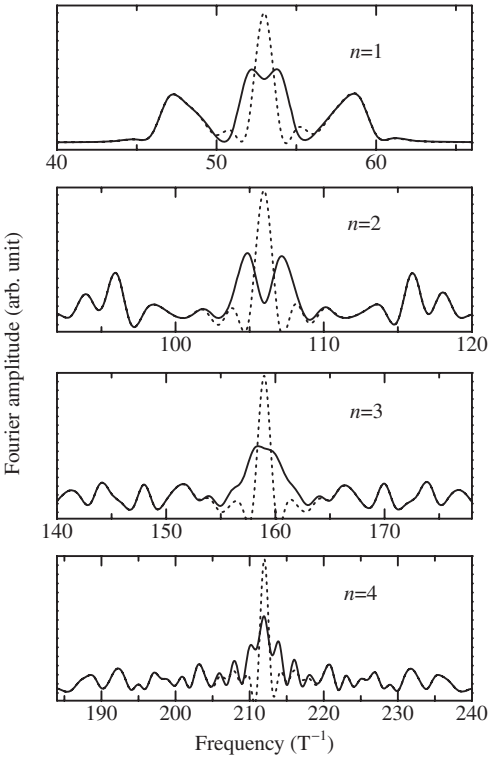

Fig. 5. Solid lines are the FT spectra of the function (4) for the winding number $n = 1, 2, 3, 4$. The magnetic field region is taken as $-0.5 < B < 0.5$ T and the parameter Δk_F is taken from SdH measurement as 4.1×10^7 m^{-1}. The scale of abscissa is modified with n to show the entire peak structures. Dotted lines are the results when Berry's phase $\Delta\theta_B$ is set to zero. Significant difference between solid and dotted lines around the center while they are almost identical in surrounding regions.

to about twice the frequency of the main peak, and originates from the orbits with the winding number $n = 2$. The signal-to-noise ratio is not high enough to resolve detailed peak structure, nevertheless the dip at C* is obvious and we may view it as a dip between two side peaks as indicated by arrows in the Fig. 3, although peak A* is not well resolved. Though there is no remarkable structure at the positions at around $n = 3$, a surprisingly clear peak is observed at the position for $n = 4$ as shown in the inset of Fig. 3.

Figure 4 displays the temperature dependence of the FT spectrum. The three peaks (A, A′, and B′) show almost identical temperature dependence as seen in the inset of Fig. 4, which can be fitted by the Dingle function,

$$f(T) \propto \frac{\kappa T}{\sinh \kappa T}, \quad \kappa \equiv \frac{2\pi^2 k_B}{\Delta E}, \tag{3}$$

where T is the temperature and ΔE the energy difference between the peaks in the density of states modulation caused by the AB effect. The fitting gives the value of ΔE as 86 μeV. This is in similar order with other measurement in 2D electron systems.[18] The agreement in the temperature dependence manifests the three peaks have the same physical origin. Here, we stress the nature of the ensemble average in AB-type oscillations in ADLs, as opposed to the ordinary AB effect in single ring structure. The AB-type oscillation manifests the oscillatory fine structure of the density of state, and the temperature dependence of the oscillation amplitude can be explained by thermal broadening of the energy levels of the orbits.

We attribute the origin of the splitting to shifts in additional phases expressed in eqs. (1) and (2). Yau *et al.*[13] introduced an expression to analyze the oscillatory resistance ΔR in an AB ring made of 2DHS as

$$\begin{aligned}\Delta R \approx & \cos(n(\theta_{AB} + \Delta\theta_B)) + \cos(n(\theta_{AB} - \Delta\theta_B)) \\ & + \cos(n(\theta_{AB} + \Delta\theta_k)) + \cos(n(\theta_{AB} - \Delta\theta_k)),\end{aligned} \tag{4}$$

where θ_{AB} is the AB phase given by $2\pi B_{ext}\pi r^2/(h/e)$. The above expression can be interpreted as follows. It is assumed that the holes are transported adiabatically along the ring. On the other hand the three-leg crossings at the ends of the ring cause mixing of l-holes and h-holes. Then the division of a hole wavefunction into two at a crossing is expressed by a selection of two points in the Fermi contours in Fig. 1(b). We consider the selection of (a, a') and that of (a, b) without loss of generality. In the former, the spins rotate in the same direction along the two paths. θ_k affects the interference while θ_B cancels each other, hence giving the third (or fourth) term in eq. (4). In the latter, θ_B is effective while θ_k is zero, which gives the first (or second) term. It is then readily to see then all possible selections gives four terms in (4). Though the discussion is for an AB ring, the same can be applied to the anti-dot system with AB-type oscillation, in which states around anti-dots are formed and the mixing of l-holes and h-holes occurs at the hopping between them.

Because the phases in eqs. (1) and (2) are not linear with respect to B_{ext}, each term in eq. (4) is not sinusoidal oscillation and hence the FT spectrum strongly depends on the region of transformation. By the same token, the FT lineshape for higher harmonics ($n > 1$) is not simply n-times enlargement in frequency axis of the main peak structure.

In order for a qualitative comparison with experiment, we calculate the FT spectra of eq. (4) in the magnetic field ranging from −0.5 to 0.5 T with $\Delta k_F = 4.1 \times 10^7$ m^{-1}, which is the value measured from the SdH oscillation, and r is taken to be $a/2$. We adopt 0.55 T for B_{eff}, which is reported for 2DHSs with conditions close to the present ones.[10] The results are shown in Fig. 5. Despite the crude approximation, the solid lines in Fig. 5 bears striking

resemblance to the experiment. For $n = 1$, clear splitting into 4 sub-peaks is observed. With increasing n, the distribution of the peaks increases but the variation of the center peak structure is not monotonic. For $n = 2$, there is a sharp dip at the center while only a broad peak exists for $n = 3$. When n is increased to 4, the peak distribution still broadens though the center peak resharpens. These non-monotonic evolutions of the shapes of FT spectra with the increase of the winding number can qualitatively describe the experiment data.

As shown by the dotted lines in Fig. 5, when there is no contribution of Berry's phase, the characteristics of the center peak are completely different. No splitting appears even for $n = 2$; Rounding and sharpening for $n = 3$ and 4 do not appear either. These results hence support the interpretation that the splitting of FT peaks is due to the phases in eqs. (1) and (2) arising from the spin–orbit coupling, added to the AB phase. Equation (4) is too crude an approximation for further quantitative discussion. Especially, in ADLs, the orbits encircling anti-dots may vary their sizes with B_{ext}, which has an effect smaller than Berry's phase and results in simple shift of peak positions. Shift of peak positions, e.g., for $n = 4$ may be explained with this effect.

We comment on the asymmetry in the peaks in FT. The peak splitting is due to the phase shift that is non-linear th respect to B_{ext} and the finite region of transformation. And the symmetry appeared in the simulation comes from the assumed symmetric MR with respect to $B_{\mathrm{ext}} = 0$. Although the device used in ref. 12 was two-terminal and should show the MR symmetric with respect to $B_{\mathrm{ext}} = 0$ due to the Onsager reciprocity, the real FT results had asymmetry, which remained as an open question. However in the present case, the device is four-terminal and quantum mechanical current density fluctuation easily causes MR asymmetry in B_{ext}. This results in the asymmetry of the peaks in FT.

One more experimental fact that supports our interpretation is that the peak splitting in the FT spectra disappears in the AB-type oscillation in high fields, where the spin is fixed perpendicular to the plane and neither variation in Berry's phase nor in Δk_{F} occurs. This phenomenon will be reported in a separate paper.

In conclusion, we have observed the significant splitting structure of Fourier transform peaks in the Aharonov–Bohm type oscillation of weak field MR in an anti-dot lattice of a two-dimensional hole system. We associate these observations with the spin–orbit Berry's phase in 2DHS with strong spin–orbit interactions. A simple simulation with adopting parameters obtained from independent measurements shows fair qualitative agreement with the experimental observations.

Acknowledgement

The authors would like to thank K. Suzuki for help during this experiment. This work is supported by a Grant-in-Aid for Scientific Research from the Ministry of Education, Culture, Sports, Science and Technology of Japan and also supported by Special Coordination Funds for Promoting Science and Technology.

1) D. Loss, P. Goldbart, and A. V. Balatsky: Phys. Rev. Lett. **65** (1990) 1655.
2) A. G. Aronov and Y. B. Lyanda-Geller: Phys. Rev. Lett. **70** (1993) 343.
3) A. Stern: Phys. Rev. Lett. **68** (1992) 1022.
4) T. Z. Qian and Z. B. Su: Phys. Rev. Lett. **72** (1994) 2311.
5) Y. Meir, Y. Gefen, and O. Entin-Wohlman: Phys. Rev. Lett. **63** (1989) 798.
6) T. Ando: J. Phys. Soc. Jpn. **54** (1985) 1528.
7) U. Ekenberg and M. Altarelli: Phys. Rev. B **30** (1984) 3569.
8) J. P. Eisenstein, H. L. Stormer, V. Narayanamurti, A. C. Gossard, and W. Wiegmann: Phys. Rev. Lett. **53** (1984) 2579.
9) H. L. Stormer, Z. Schlesinger, A. Chang, D. C. Tsui, A. C. Gossard, and W. Wiegmann: Phys. Rev. Lett. **51** (1983) 126.
10) J. P. Lu, J. B. Yau, S. P. Shukla, and M. Shayegan: Phys. Rev. Lett. **81** (1998) 1282.
11) Y. Iye, E. E. Mendez, W. I. Wang, and L. Esaki: Phys. Rev. B **33** (1986) 5854.
12) A. F. Mopurgo, J. P. Heida, T. M. Klapwijk, B. J. van Wees, and G. Borghs: Phys. Rev. Lett. **80** (1998) 1050.
13) J.-B. Yau, E. P. De Poortere, and M. Shayegan: Phys. Rev. Lett. **88** (2002) 146801.
14) M. J. Yang, C. H. Yang, and Y. B. Lyanda-Geller: Europhys. Lett. **66** (2004) 826.
15) D. Weiss, K. Richter, A. Menschig, R. Bergmann, H. Schweizer, K. von Klitzing, and G. Weimann: Phys. Rev. Lett. **70** (1993) 4118.
16) See for review, e.g., T. Ando, S. Uryu, S. Ishizaka, and T. Nakanishi: Chaos Solitons Fractals **8** (1997) 1057.
17) F. Nihey and K. Nakamura: Physica B **184** (1993) 398.
18) Y. Iye, M. Ueki, A. Endo, and S. Katsumoto: J. Phys. Soc. Jpn. **73** (2004) 3370.